

Rowan University

## Rowan Digital Works

---

Faculty Scholarship for the College of Science & Mathematics

College of Science & Mathematics

---

11-6-2023

# Effect of Hf alloying on magnetic, structural, and magnetostrictive properties in FeCo films for magnetoelectric heterostructure devices

Thomas Mion

Margo Staruch

Konrad Bussmann

Goran Karapetrov

Olaf van 't Erve

*See next page for additional authors*

Follow this and additional works at: [https://rdw.rowan.edu/csm\\_facpub](https://rdw.rowan.edu/csm_facpub)



Part of the [Materials Science and Engineering Commons](#), and the [Physics Commons](#)

---

### Recommended Citation

Thomas Mion, Margo Staruch, Konrad Bussmann, Goran Karapetrov, Olaf van 't Erve, Sara Mills, Heonjune Ryou, Ramasis Goswami, Patrick G. Callahan, David J. Rowenhorst, Syed B. Qadri, Samuel E. Lofland, Peter Finkel; Effect of Hf alloying on magnetic, structural, and magnetostrictive properties in FeCo films for magnetoelectric heterostructure devices. APL Mater. 1 November 2023; 11 (11): 111107. <https://doi.org/10.1063/5.0168112>

This Article is brought to you for free and open access by the College of Science & Mathematics at Rowan Digital Works. It has been accepted for inclusion in Faculty Scholarship for the College of Science & Mathematics by an authorized administrator of Rowan Digital Works.














---

## Authors

Thomas Mion, Margo Staruch, Konrad Bussmann, Goran Karapetrov, Olaf van 't Erve, Sara Mills, Heonjune Ryou, Ramasis Goswami, Patrick G. Callahan, David J. Rowenhorst, Syed B. Qadri, Samuel Lofland, and Peter Finkel

RESEARCH ARTICLE | NOVEMBER 06 2023

## Effect of Hf alloying on magnetic, structural, and magnetostrictive properties in FeCo films for magnetoelectric heterostructure devices

Thomas Mion ; Margo Staruch ; Konrad Bussmann ; Goran Karapetrov ; Olaf van 't Erve ; Sara Mills ; Heonjune Ryou ; Ramasis Goswami; Patrick G. Callahan ; David J. Rowenhorst ; Syed B. Qadri ; Samuel E. Lofland ; Peter Finkel  



*APL Mater.* 11, 111107 (2023)

<https://doi.org/10.1063/5.0168112>



CrossMark



**Biomicrofluidics**  
Special Topic:  
Microfluidic Biosensors  
**Submit Today**

# Effect of Hf alloying on magnetic, structural, and magnetostrictive properties in FeCo films for magnetoelectric heterostructure devices

Cite as: APL Mater. 11, 111107 (2023); doi: 10.1063/5.0168112

Submitted: 17 July 2023 • Accepted: 6 October 2023 •

Published Online: 6 November 2023



Thomas Mion,<sup>1</sup> Margo Staruch,<sup>2</sup> Konrad Bussmann,<sup>2</sup> Goran Karapetrov,<sup>3</sup> Olaf van 't Erve,<sup>2</sup> Sara Mills,<sup>1</sup> Heonjune Ryou,<sup>2</sup> Ramasis Goswami,<sup>2</sup> Patrick G. Callahan,<sup>2</sup> David J. Rowenhorst,<sup>2</sup> Syed B. Qadri,<sup>2</sup> Samuel E. Lofland,<sup>4</sup> and Peter Finkel<sup>2,a)</sup>

## AFFILIATIONS

<sup>1</sup>American Society for Engineering Education Postdoc Fellow at US Naval Research Laboratory, Washington, DC 02375, USA

<sup>2</sup>US Naval Research Laboratory, Washington, DC 02375, USA

<sup>3</sup>Department of Physics, Drexel University, Philadelphia, Pennsylvania 19104, USA

<sup>4</sup>Department of Physics and Astronomy, Rowan University, Glassboro, New Jersey 08028, USA

<sup>a)</sup>Author to whom correspondence should be addressed: [peter.finkel@nrl.navy.mil](mailto:peter.finkel@nrl.navy.mil)

## ABSTRACT

Materials with high magnetoelectric coupling are attractive for use in engineered multiferroic heterostructures with applications such as ultra-low power magnetic sensors, parametric inductors, and non-volatile random-access memory devices. Iron-cobalt alloys exhibit both high magnetostriction and high saturation magnetization that are required for achieving significantly higher magnetoelectric coupling. We report on sputter-deposited  $(\text{Fe}_{0.5}\text{Co}_{0.5})_{1-x}\text{Hf}_x$  ( $x = 0 - 0.14$ ) alloy thin films and the beneficial influence of Hafnium alloying on the magnetic and magnetostrictive properties. We found that co-sputtering Hf results in the realization of the peening mechanism that drives film stress from highly tensile to slightly compressive. Scanning electron microscopy and x-ray diffraction along with vibrating sample magnetometry show reduction in coercivity with Hf alloying that is correlated with reduced grain size and low film stress. We demonstrate a crossover from tensile to compressive stress at  $x \sim 0.09$  while maintaining a high magnetostriction of 50 ppm and a low coercive field of 1.1 Oe. These characteristics appear to be related to the amorphous nature of the film at higher Hf alloying.

© 2023 Author(s). All article content, except where otherwise noted, is licensed under a Creative Commons Attribution (CC BY) license (<http://creativecommons.org/licenses/by/4.0/>). <https://doi.org/10.1063/5.0168112>

## I. INTRODUCTION

Materials that possess high magnetostriction and low coercive fields have wide ranging applications, including actuators, magnetic field sensors, gyrators, and transformers, and have been employed extensively in multiferroic systems displaying high magnetoelectric coupling.<sup>1–6</sup> In artificial magnetoelectric systems built on the combination of ferromagnetic magnetostrictive materials structurally coupled to piezoelectric and ferroelectric materials, the desired magnetic properties often require implementation of a soft magnetic material with large magnetostriction to produce a high piezomagnetic response that is directly proportional to the magnetoelectric coupling coefficient. Magnetoelectric microelectromechanical systems (ME-MEMS) are used to construct devices such as ultra-low

power magnetometers, miniaturized antennas, and high-quality resonator heterostructures and are amenable to well-developed processing techniques, including magnetron sputtering<sup>7–10</sup> for film deposition. Requirements for device fabrication often complicate the realization of these combined qualities as inherent stresses from the deposition technique are often detrimental to the magnetoelectric functionality. Solutions to these problems are rarely reported.

$\text{Fe}_{1-y}\text{Co}_y$  (FeCo) alloys are broadly used in thin-film form and have been widely studied for their magnetoelastic properties and suitability for technological integration.<sup>10,11</sup> FeCo alloys have some of the highest saturation magnetization values available and can be alloyed to create soft magnetic materials desirable for numerous applications.<sup>12,13</sup> For example,  $\text{Fe}_{0.5}\text{Co}_{0.5}$  has an extraordinary saturation magnetization of 2.45 T, which is the highest value of all

magnetic materials at room temperature per the Slater–Pauling rule.  $\text{Fe}_{0.5}\text{Co}_{0.5}$  stabilizes in a bcc structure with low magnetic anisotropy, high magnetostriction, and high Curie temperature that coincides with the bcc-to-fcc transition temperature ( $\sim 985^\circ\text{C}$ ). It is noteworthy that in FeCo systems, the crystalline anisotropy and saturation magnetostriction  $\lambda_s$  have minima at different Co concentrations, allowing compositions to be optimized to these parameters. Multiple ferromagnet–metalloid alloy films have been investigated in recent years as the incorporation of C, B, Si, N, and mixtures thereof within the FeCo parent alloy reduces grain size and promotes the formation of an amorphous phase, which leads to decreased coercive field  $H_c$  while retaining high  $\lambda_s$  and piezomagnetic coefficients  $d_{ij}$ .<sup>14–18</sup>

Magnetic and magnetoelastic properties of magnetostrictive thin films used in ME-MEMS are significantly impacted by the inherent stress of the film imparted during deposition, leading to a stress-induced magnetic anisotropy.<sup>19–22</sup> Even more fundamental are the intrinsic properties linked to the stresses of the magnetostrictive layers, where a direct correlation between the stress state,  $\lambda_s$ , and  $d_{ij}$  can be found.<sup>23</sup> *In situ* deposition parameters, such as pressure and stage bias voltages, are possible means of controlling the as-deposited stress in magnetic thin films.<sup>24</sup> Additionally, deposition of materials with higher atomic mass also tends to go down under compression, so introduction of higher-Z elements may also assist with tuning of the intrinsic stress via the peening mechanism.<sup>25</sup> Although previous studies have shown that the co-deposition of Hf with FeCo can lead to amorphization, resulting in magnetically soft films with compressive stress and good microwave magnetic properties,<sup>26–29</sup> none has explored how the Hf content can modulate the film stress or magnetoelastic properties. In this work, we analyze  $(\text{Fe}_{0.5}\text{Co}_{0.5})_{1-x}\text{Hf}_x$  thin films ( $0 \leq x \leq 0.14$ ) and the correlations between the alloying and the structural amorphization, the as-deposited film stress, and various magnetic properties. We demonstrate that stress can be varied with Hf alloying via a mechanism typically achieved with low-Z metalloids. Such films with tunable stress that maintain high magnetostriction are critical for the development of next generation magnetic MEMS devices.

## II. EXPERIMENTAL

Films of  $(\text{Fe}_{0.5}\text{Co}_{0.5})_{1-x}\text{Hf}_x$  were grown by magnetron sputtering with commercially available targets from ACI Alloys. Hf, by nature of the high atomic mass, is chosen to modulate the film stress via the peening mechanism. Depositions were performed in an AJA International, Inc. Orion confocal sputtering system configured with 2 in. diameter sputtering guns. The magnetic FeCo target was mounted in the flux concentrator configuration, and the Hf target was mounted in the unbalanced configuration. The target to substrate distance was  $\sim 20$  cm.  $\text{Fe}_{0.5}\text{Co}_{0.5}$  was deposited with a pulsed DC power supply (100 W/100 kHz, 2  $\mu\text{s}$ ), and Hf was co-sputtered with an RF supply to allow for low film concentrations. The RF power supply power levels were varied from 0 to 24 W for deposition of the Hf films, resulting in an alloying range of 0%–14% at. Films were co-sputtered on 100- $\mu\text{m}$  thick (001) Si disk substrates cut into 18 mm circular disks suspended with a recessed ring, allowing the film to be grown on a non-strained substrate. In addition, films were also deposited on an accompanying cover slip dotted with photoresist to allow for step height measurement of film thickness by surface profilometry. The system base pressure was lower

than  $2.0 \times 10^{-8}$  Torr, and deposition was performed with Ar gas at a pressure of 2.0 mTorr. Lower pressure operation did not allow stable plasma during the extent of the deposition, which prevented the low-pressure approach to induce compressive stress. A 10-nm Ti adhesion layer was initially sputtered on the Si disk, and then,  $\sim 230$  nm of FeCo–Hf was deposited.

Stress measurements were determined by use of a Zygo NewView 7200 white light interferometer to image the full 18-mm diameter disk and determine the radius of curvature induced by film stress. Stoney's formula<sup>30</sup> was used in combination with thickness measurements to determine the film stress. Composition was determined by energy dispersive x-ray spectroscopy (EDS) done with an Oxford AZTEC spectrometer mounted on a LEO Supra scanning electron microscope (SEM). EDS also consistently showed that the actual deposition of FeCo was close to  $\text{Fe}_{0.47}\text{Co}_{0.53}$  independent of the Hf content. Electron backscatter diffraction (EBSD) data were collected on a ThermoFisher Quattro S scanning electron microscope with an accelerating voltage of 20 kV and a beam current of 4.2 nA with an EDAX Velocity Super EBSD detector. The EBSD patterns from each dataset were denoised by the non-local means pattern averaging re-indexing (NLPAR) technique<sup>31</sup> with a fitting parameter  $\lambda_{\text{EBSD}} = 1.33$  and a search window of 7 prior to re-indexing. X-ray diffraction was performed with a Rigaku SmartLab x-ray powder diffractometer to investigate the structural properties of the as-deposited films in a  $\theta$ – $2\theta$  geometry with Cu- $K_\alpha$  (1.54 Å) radiation at 50 kV and 200 mA. A Thermo Scientific SEM operating at 30 kV was used to obtain micrographs for grain analysis with an Everhart–Thornley detector (ETD) and a circular backscatter (CBS) detector, each with resolutions of  $\sim 7$  nm. Nanoindentation hardness tests were made with a Berkovich indenter on an NHT2 Anton Paar Nano Indenter at a maximum load of 5 mN with a standard linear loading to determine Young's modulus.

Magnetic measurements were performed with a Lakeshore 7400 vibrating sample magnetometer (VSM) to trace in-plane magnetic hysteresis loops. Magnetic force microscopy (MFM) done with a Bruker Multimode 8 with Nanoscope V SPM Controller and MESP (Veeco) magnetic probes (hard Co–Cr coating, tip radius  $\sim 30$  nm, and resonant frequency  $\sim 75$  kHz) was conducted to investigate the magnetic domains. MFM scans were performed in interleave tapping mode — after a trace/retrace tapping mode line scan, a second interleave scan was taken with a 30-nm height offset (“lift mode”) to eliminate the van der Waals interaction and assess the magnetic interaction between the magnetic moment of the tip and the local stray fields of the sample. The MFM images were obtained in the phase mode, and before each measurement, the tip was magnetized perpendicular to the surface of the thin film. Magneto Optic Kerr Effect (MOKE) measurements were performed using a NanoMOKE3 from Durham Magneto Optics with samples mounted in the longitudinal configuration.

## III. RESULTS AND DISCUSSION

### A. Structural Properties

XRD analysis of  $(\text{Fe}_{0.5}\text{Co}_{0.5})_{1-x}\text{Hf}_x$  is shown in Fig. 1(a) where the  $\text{Fe}_{0.5}\text{Co}_{0.5}$  bcc (110) peak is pronounced in pure FeCo films and shifts to lower  $2\theta$  and broadens with increasing Hf concentration, indicating a distortion of the lattice constant and accompanied by a progressive reduction in grain size. A broad peak

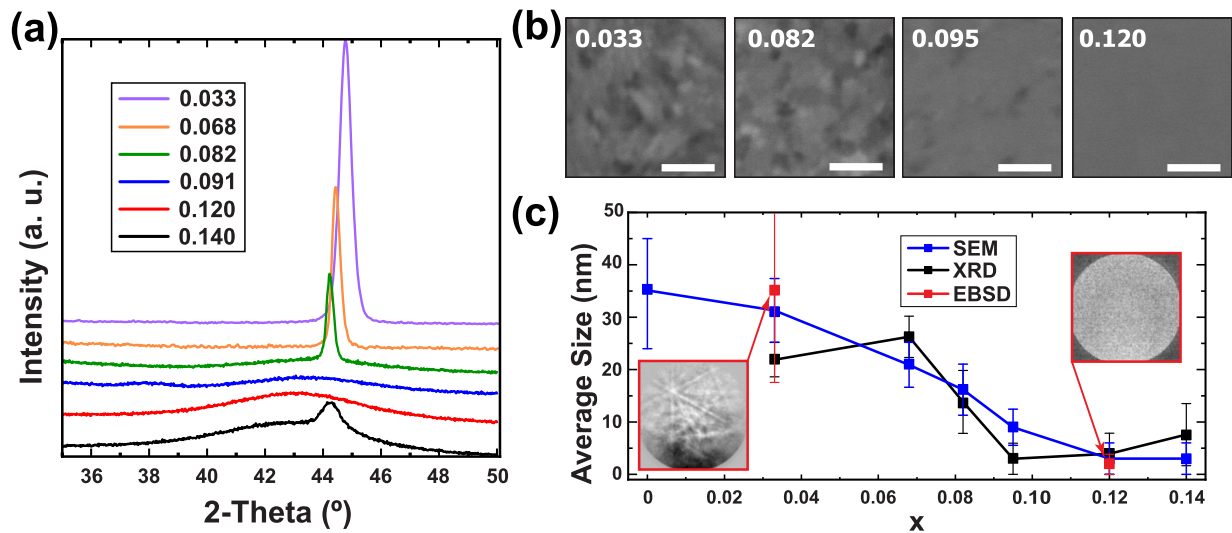


**FIG. 1.** Structural properties of  $(\text{Fe}_{0.5}\text{Co}_{0.5})_{1-x}\text{Hf}_x$  thin films. (a) X-ray diffraction patterns spanning the (110) peak for  $x = 0.033$ – $0.14$  with intensities of  $x = 0.068$  scaled by  $6\times$  and  $x = 0.082$ – $0.140$  scaled by  $20\times$ . (b) SEM images with scale bars representing 100 nm with CBS detector. (c) Summary of the average grain (SEM and EBSD) and crystallite (XRD) sizes with insets showing example EBSD patterns for  $x = 0.033$  and  $x = 0.120$ .

begins to form as  $x$  approaches 0.07, which signals a reduction in the crystallite size and potentially the onset of an amorphous phase. This possibly amorphous phase dominates for larger  $x$  values with a re-emergence of a crystalline phase at  $x = 0.14$ . As this additional peak is close to Co (111), additional XRD scans over a broad range were performed and outlined in Fig. S1 whereby an additional peak at  $\sim 97^{\circ}$  leads to the conclusion that this incipient phase is a precipitation of cobalt at higher alloy content. Average crystallite sizes were estimated from the Scherrer equation and summarized in Fig. 1(c) with a notable minimum around  $x = 0.095$ . Analysis of the peaks was performed by fitting the peaks with a Gaussian function to obtain FWHM and error bars. At  $x = 0.14$ , the appearance of peaks from both the possibly amorphous phase and incipient crystalline phase makes it difficult to define an average grain size.

Characteristic images of the sample topography with the SEM CBS detector are illustrated in Fig. 1(b) for selected samples where a progressive decrease in grain size with increasing  $x$  is evident, reaching instrumental resolution by  $x = 0.12$ . The ETD and CBS micrographs were analyzed with ImageJ to determine the average grain sizes for a field of view of  $700 \text{ nm}^2$  at a magnification of  $250\,000\times$ . Figure 1(c) shows the grain size reduction with increased  $x$  and correlates well with crystallite size found by XRD discussed previously. SEM imaging of the grains for  $x = 0.033$  reveals the presence of elongated grains with higher aspect ratios than those seen at higher  $x$ . Further analysis is shown in Fig. S2(a) regarding the grain size and shape where characteristic images over the same field of view obtained simultaneously with ETD and CBS detectors show the aggregation of multiple crystallites into a single grain. Example EBSD patterns for  $x = 0.033$  and  $x = 0.120$  are shown in Fig. 1(c) as insets. The small grain size in  $x = 0.033$  leads to the production of EBSD patterns with Kikuchi bands from multiple grain overlapping. This pattern overlap made it difficult or impossible to unambiguously index the Kikuchi patterns from all but the largest grains in

the sample. The grains that were large enough to produce indexable Kikuchi patterns had a body centered cubic crystal structure and were on the order of 50–100 nm. The Kikuchi patterns from  $x = 0.120$  showed no evidence of crystallinity, that is, no Kikuchi bands or zone axis contrast was evident, and the patterns were simply uncorrelated noise. Inverse pole figure EBSD maps of  $x = 0.033$ , which contains grains on the scale of 10s of nm and  $x = 0.12$  where there was no evidence of crystallinity, are shown in Fig. S2(b).

## B. Magnetic and Stress Properties

Figure 2(a) shows  $5 \times 5 \mu\text{m}^2$  MFM images that were obtained in ambient conditions without the application of an external magnetic field. Considering the nominal tip radius and the lift height, we estimate the lateral MFM resolution to be  $\sim 30 \text{ nm}$ . Subsequent analysis of the magnetic domain shapes and sizes shows a progression of domains from 370 nm round domains at  $x = 0.033$  to predominantly stripe domains present at  $x = 0.068$  with width  $\sim 480 \text{ nm}$ . MFM images of  $x = 0.082$  reveal the existence of large, nonuniform domains with stripe widths between 450 nm– $1 \mu\text{m}$ . For  $0.09 < x < 0.12$ , no domains were observed on the scale measured. Likely, the magnetically soft samples possess domains that are significantly larger than the field of view. Finally,  $x = 0.14$  shows clear stripe domains with periodicity  $\sim 390 \text{ nm}$ . This is consistent with an expected out-of-plane easy axis for positive  $\lambda_s$  and large compressive in-plane stress, which forces the magnetization out-of-plane, while the demagnetization of the thin films forces the magnetization in-plane, and it is this competition between demagnetization energy and stress-induced anisotropy that gives rise to stripe domains. Magnetization measurements along the easy axis detailed in Fig. 2(b) show the lowest coercive field  $H_c$  of only 1.1 Oe for  $x = 0.091$ , which is also the value where the loop is the most square. These observations are likely tied to the absence of magnetocrystalline anisotropy



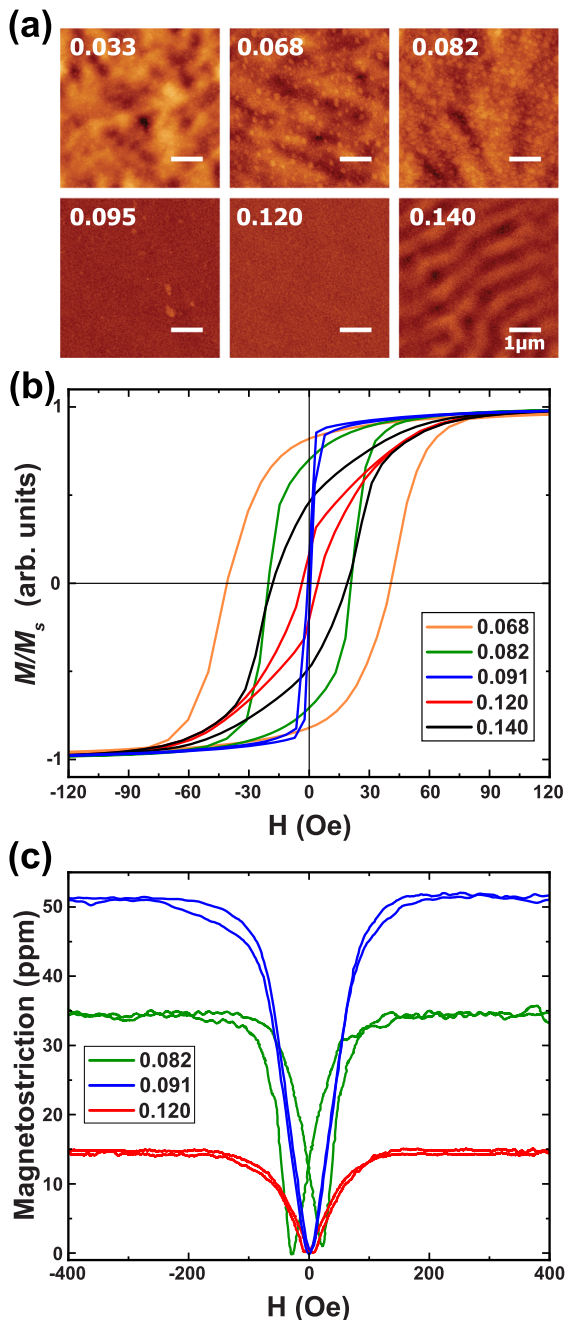


**FIG. 2.** (a) MFM images of magnetic domains, (b) normalized in-plane magnetization curves measured by VSM, and (c) magnetostriction of selected samples.

in the possibly amorphous phase, whereas the lower alloy content promotes a polycrystalline phase, which still retains small anisotropy values. Polycrystalline samples often have larger  $H_c$  due to the variation in the local magnetic easy axis, which also can distort the shape of the loop from square.

After analytical and magnetic measurements were performed, the Si disk was laser scribed to fabricate an  $18 \times 2$  mm beam on which to perform magnetostrictive measurements by the cantilever method.<sup>13,32,33</sup> Measurements were taken for orthogonal in-plane directions to determine the saturation magnetostriction  $\lambda_s$  and the displacement of the cantilever was determined from laser Doppler vibrometry while sweeping the magnetic field up to 1.5 kOe. A trend similar to the progression of  $H_c$  is reflected in the magnetostriction data, as seen in Fig. 2(c). To determine  $\lambda_s$ , the reduced modulus  $Y^*$  for  $x = 0.091$  was investigated with nanoindentation hardness tests, giving a value of  $170 \pm 10$  GPa (see details in Fig. S3 of the supplementary material).  $\lambda_s$  for all other samples was estimated based on that same value for  $Y^*$ . In general,  $\lambda_s$  increases as the films become increasingly amorphous up to  $x = 0.095$  and reduces with further alloying.

A summary of the magnetic and magnetostrictive properties is plotted in Fig. 3 and shows a striking similarity to the case of  $(\text{Fe}_{0.5}\text{Co}_{0.5})_{1-x}\text{C}_x$  thin films in terms of the trends in  $H_c$ ,  $\lambda_s$ , and piezomagnetic coefficient  $d_{33}$ .<sup>18</sup> As expected, the saturation magnetization  $M_s$  [Fig. 3(b)] generally decreases with  $x$  due to magnetic dilution.  $\lambda_s$  increases with  $x$  until the onset of amorphization, reaching a maximum coincident with the minimum in  $H_c$  at  $x = 0.091$ . It is of note that the trend in  $d_{33}$  and maximum in  $\lambda_s$ , as seen in Fig. 3(d), is similar to the results of  $(\text{Fe}_{0.5}\text{Co}_{0.5})_{1-x}\text{C}_x$ , in which a peak in  $\lambda_s$  occurs at a slightly higher  $x$  value than that of the maximum value of  $d_{33}$ .<sup>18</sup>

As-deposited film stresses are plotted in Fig. 3(e). Characteristic Zygo profilometer images for  $x = 0$  and 0.091 are inset in

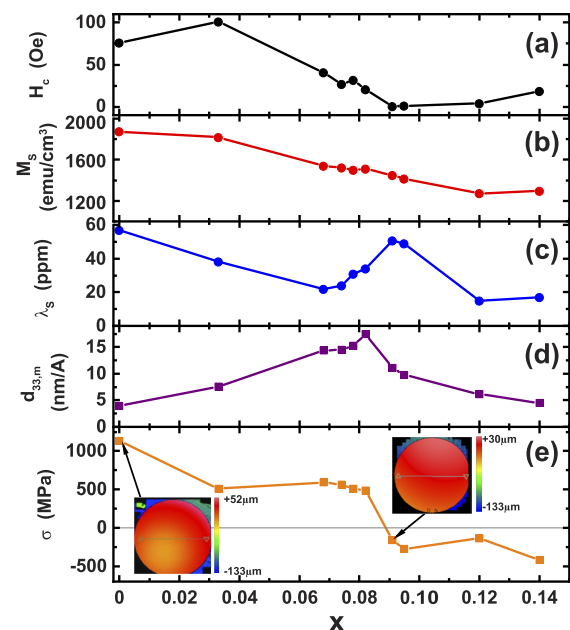


**FIG. 3.** Summary of magnetic and stress properties of  $(\text{Fe}_{0.5}\text{Co}_{0.5})_{1-x}\text{Hf}_x$  thin films: (a) coercive field  $H_c$ , (b) saturation magnetization  $M_s$ , (c) saturation magnetostriction  $\lambda_s$ , (d) piezomagnetic constant  $d_{33}$ , and (e) average stress  $\sigma$  of the as-deposited films with the color insets showing the change in substrate height due to curvature data for  $x = 0$  and 0.091.

Fig. 3(e) with scale bars for the false color image illustrating the magnitude of surface curvature. The parent ( $\text{Fe}_{0.5}\text{Co}_{0.5}$ ) films show tensile stresses  $>1$  GPa, whereas the introduction of Hf reduces the intrinsic stress by a factor of two and remains fairly constant until  $x \sim 0.085$ . Here, we use the convention where positive values represent tensile stresses and negative values represent compressive ones. A clear crossover from tensile to compressive stress occurs at  $x \sim 0.09$ , which corresponds to the minimum in  $H_c$  and maximum in  $\lambda_s$  with only a slightly reduced value of  $d_{33}$ .

Figure 4(a) shows the normalized MOKE measurements  $M_x(H)/M_s$  for various samples near the easy axis, which is representative of the trend seen in VSM measurements (both MOKE and VSM measured in plane). Figure 4(b) shows the in-plane results for  $M_x(H)/M_s$  along the hard and easy axes for  $x = 0.091$  where the stress-induced magnetic anisotropy field of 66 Oe is determined from the intersection of the extrapolation of the low-field linear region to magnetic saturation (blue dashed line). The green line in

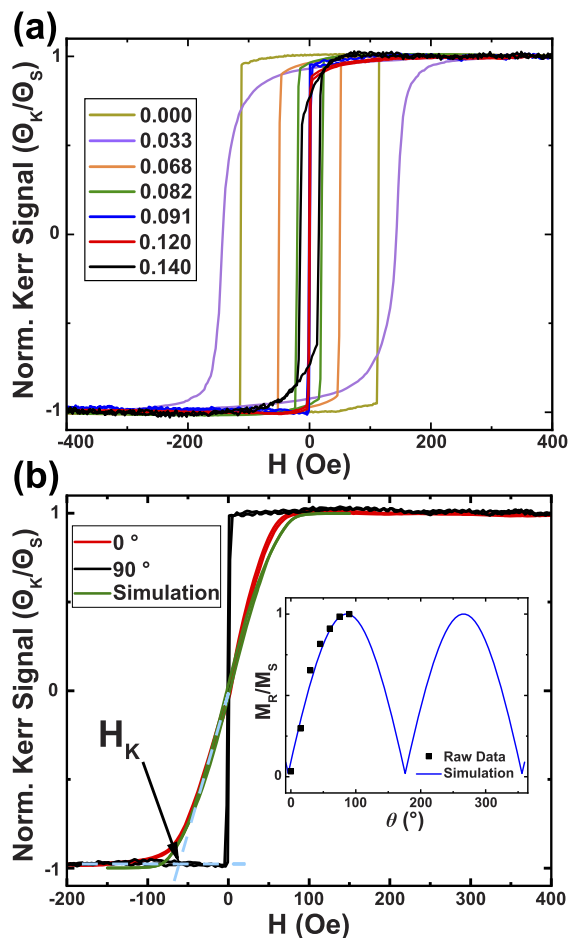


**FIG. 4.** (a) Normalized MOKE signals for various Hf alloying. (b) MOKE signal for easy (black) and hard (red) axis for  $x = 0.091$  with the inset showing magnetization. The green line represents the calculated magnetization along the hard axis based on Eq. (1) and the parameters determined from the high-field torque measurements.

the figure represents the expected calculated magnetization along the hard axis based on Eq. (1) and the values determined from the high-field torque measurements. The agreement with the measurement is quite satisfactory. Note that the inset shows the measured and calculated remanence, given by  $M_x/M_s$  at  $H = 0$ .

Vector magnetic measurements were performed for  $x = 0.091$  by VSM by measuring  $M_x$  and  $M_y$ , where  $M_x$  is the component of  $\mathbf{M} \parallel \mathbf{H}$  and  $M_y$  is the component of  $\mathbf{M} \perp \mathbf{H}$ . The sample was measured at every  $5^\circ$  in the plane, and measurements were averaged between the opposite orientations. Figure S4(a) shows the  $M-H$  loops for  $M_x$  and  $M_y$  near the easy axis, and Fig. S4(b) shows the angular dependence of  $M_y$  measured at 1500 Oe (black squares). Given that the MFM images indicated large domains for this composition, the results were modeled by minimizing the free energy for a single domain isotropic ferromagnet,

$$F = -M_s H_i \alpha_i + \frac{1}{2} \alpha_i \alpha_j D_{ij} - \frac{Y}{2(1+\nu)} \times \left[ 3\lambda_s \left( \alpha_i \alpha_j \varepsilon_{ij} - \frac{1}{3} \varepsilon_{ii} \right) + \varepsilon_{ij} \varepsilon_{ij} + \frac{\nu}{(1-2\nu)} \varepsilon_{ii} \varepsilon_{jj} \right] - \sigma_{ij} \varepsilon_{ij}, \quad (1)$$

where  $H_i$  is the magnetic field,  $\alpha_i$  is the direction cosine of the magnetization,  $D_{ij}$  is the demagnetization tensor,  $Y$  is Young's modulus,  $\nu$  is the Poisson ratio,  $\varepsilon_{ij}$  is the strain tensor, and  $\sigma_{ij}$  is the deposition stress tensor.  $Y = (1 - \nu^2)Y^*$ , and an expected value for  $\nu$  for most metals is  $\sim 0.3$ . If we set the index "3" direction to be the surface normal, then  $D_{ij} = 0$  except  $D_{33} = 4\pi$  for a thin film. This large demagnetizing term implies that  $\alpha_3 = 0$ . Since the top surface of the film is free,  $\sigma_{33} = 0$ , and we assume that there are no shear stresses:  $\sigma_{ij} = 0$ ,  $i \neq j$ . The average deposition stress is  $-160$  MPa  $= \frac{1}{2}(\sigma_{11} + \sigma_{22})$ . The best fit yields the result shown in Fig. S4(b) with  $\sigma_{11} = -192$  MPa and  $\sigma_{22} = -128$  MPa. The in-plane anisotropy field is given by  $\frac{3\lambda_s(\sigma_{11} - \sigma_{22})}{M_s} = 66$  Oe. A similar analysis of  $x = 0.14$  was made with the data shown in Fig. S5 where fitting results with  $\sigma_{11} = -451$  MPa and  $\sigma_{22} = -427$  MPa, consistent with stress measured via Zygo profilometry.

#### IV. CONCLUSIONS

In conclusion, we have investigated  $(\text{Fe}_{0.5}\text{Co}_{0.5})_{1-x}\text{Hf}_x$  thin films made by co-sputtering Hf and FeCo. We find that a sharp transition from tensile to compressive stress is observed with increased Hf concentration. At the crossover from tensile to compressive stress ( $x \sim 0.09$ ), the coercive field is small ( $\sim 1$  Oe), while the saturation magnetostriction is at a maximum. While the low coercive field and perhaps the magnitude of the residual stress can be connected to the amorphization of the film, which occurs at this critical value, it seems serendipitous that magnetostriction is also largest at this value. It should be noted the impact of various deposition conditions, such as target to substrate distance, deposition pressure, substrate bias, and substrate temperature, were not explored yet could prove beneficial as an additional control for tuning the as-deposited properties. Nonetheless, by alloying Hf with FeCo, one can enhance the piezomagnetic properties without compromising other magnetic characteristics. This material presents an additional avenue toward optimizing the design of multiferroic magnetoelectric magnetic field sensors<sup>34</sup> and broadening the application of magnetoelectric heterostructure systems.



## SUPPLEMENTARY MATERIAL

Additional characterization of samples by x-ray diffraction, scanning electron microscopy, nanoindentation, electron backscatter diffraction, and vector vibrating sample magnetometry are given in the supplementary material.

## ACKNOWLEDGMENTS

This work was supported by the U.S. Office of Naval Research through the Naval Research Laboratory's basic research program. T.M. and S.M. would like to acknowledge the support of the American Society for Engineering Education and the U.S. Naval Research Laboratory postdoctoral fellowship program.

## AUTHOR DECLARATIONS

### Conflict of Interest

The authors have no conflicts to disclose.

## Author Contributions

**Thomas Mion:** Conceptualization (equal); Data curation (lead); Formal analysis (lead); Investigation (lead); Methodology (equal); Writing – original draft (lead); Writing – review & editing (equal). **Margo Staruch:** Formal analysis (equal); Funding acquisition (equal); Investigation (supporting); Writing – original draft (equal). **Konrad Bussmann:** Conceptualization (equal); Investigation (equal); Writing – original draft (equal). **Goran Karapetrov:** Investigation (equal). **Olaf van't Erve:** Investigation (equal). **Sara Mills:** Investigation (supporting). **Heonjune Ryou:** Investigation (equal). **Ramasis Goswami:** Investigation (equal). **Patrick G. Callahan:** Investigation (supporting). **David J. Rowenhorst:** Investigation (supporting). **Syed B. Qadri:** Investigation (equal). **Samuel E. Lofland:** Formal analysis (equal); Writing – original draft (equal). **Peter Finkel:** Conceptualization (equal); Formal analysis (equal); Funding acquisition (lead); Methodology (equal); Project administration (lead); Supervision (equal); Writing – original draft (equal).

## DATA AVAILABILITY

The data that support the findings of this study are available from the corresponding author upon reasonable request.

## REFERENCES

- D. Howe, "Magnetic actuators," *Sens. Actuators, A* **81**(1–3), 268–274 (2000).
- J. Gao, Z. Jiang, S. Zhang, Z. Mao, Y. Shen, and Z. Chu, "Review of magnetoelectric sensors," *Actuators* **10**(6), 109 (2021).
- S. Marauska, R. Jahns, H. Greve, E. Quandt, R. Knöchel, and B. Wagner, "MEMS magnetic field sensor based on magnetoelectric composites," *J. Micromech. Microeng.* **22**, 065024 (2012).
- X. Zhuang, C. Dolabdjian, C. M. Leung, J. Xu, J. Zhang, G. Srinivasan, J. Li, and D. Viehland, "Dimension effects of a magnetoelectric gyator with FeCoSiB/Pb(Zr,Ti)O<sub>3</sub> layered composites core for efficient power conversion," *Sens. Actuators, A* **302**, 111815 (2020).

- S. Bhuktare, A. Bose, H. Singh, and A. A. Tulapurkar, "Gyrator based on magneto-elastic coupling at a ferromagnetic/piezoelectric interface," *Sci. Rep.* **7**(1), 840 (2017).
- D. K. Pradhan, S. Kumari, and P. D. Rack, "Magnetoelectric composites: Applications, coupling mechanisms, and future directions," *Nanomaterials* **10**(10), 2072 (2020).
- S. P. Bennett, J. W. Baldwin, M. Staruch, B. R. Matis, J. LaComb, O. M. J. van't Erve, K. Bussmann, M. Metzler, N. Gottron, W. Zappone, R. LaComb, and P. Finkel, "Magnetic field response of doubly clamped magnetoelectric microelectromechanical AlN-FeCo resonators," *Appl. Phys. Lett.* **111**, 252903 (2017).
- C. Tu, Z.-Q. Chu, B. Spetzler, P. Hayes, C.-Z. Dong, X.-F. Liang, H.-H. Chen, Y.-F. He, Y.-Y. Wei, I. Lisenkov, H. Lin, Y.-H. Lin, J. McCord, F. Faupel, E. Quandt, and N.-X. Sun, "Mechanical-resonance-enhanced thin-film magnetoelectric heterostructures for magnetometers, mechanical antennas, tunable RF inductors, and filters," *Materials* **12**(14), 2259 (2019).
- S. Zabel, C. Kirchhof, E. Yarar, D. Meyners, E. Quandt, and F. Faupel, "Phase modulated magnetoelectric delta-E effect sensor for sub-nano tesla magnetic fields," *Appl. Phys. Lett.* **107**, 152402 (2015).
- X. Liang, A. Matyushov, P. Hayes, V. Schell, C. Dong, H. Chen, Y. He, A. Will-Cole, E. Quandt, P. Martins, J. McCord, M. Medarde, S. Lanceros-Méndez, S. Van Dijken, N. X. Sun, and J. Sort, "Roadmap on magnetoelectric materials and devices," *IEEE Trans. Magn.* **57**(8), 400157 (2021).
- M. Staruch, S. P. Bennett, B. R. Matis, J. W. Baldwin, K. Bussmann, D. B. Gopman, Y. Kabanov, J. W. Lau, R. D. Shull, E. Langlois, C. Arrington, J. R. Pillars, and P. Finkel, "Magnetoelectric effects in doubly clamped electroplated Co<sub>77</sub>Fe<sub>23</sub> microbeam resonators," *Phys. Rev. Appl.* **11**(3), 034028 (2019).
- R. S. Sundar and S. C. Deevi, "Soft magnetic FeCo alloys: Alloy development, processing, and properties," *Int. Mater. Rev.* **50**(3), 157–192 (2013).
- D. Hunter, W. Osborn, K. Wang, N. Kazantseva, J. Hatrick-Simpers, R. Suchoski, R. Takahashi, M. L. Young, A. Mehta, L. A. Bendersky, S. E. Lofland, M. Wuttig, and I. Takeuchi, "Giant magnetostriction in annealed Co<sub>1-x</sub>Fe<sub>x</sub> thin-films," *Nat. Commun.* **2**(1), 518 (2011).
- M. Munakata, M. Namikawa, M. Motoyama, M. Yagi, Y. Shimada, M. Yamaguchi, and K.-I. Arai, "Magnetic properties and frequency characteristics of (CoFeB)<sub>x</sub>-(SiO<sub>1.9</sub>)<sub>x</sub> and CoFeB films for RF application," *Trans. Magn. Soc. Jpn.* **2**(5), 388–393 (2002).
- M. Munakata, S. I. Aouki, and M. Yagi, "B-concentration dependence on anisotropy field of CoFeB thin film for gigahertz frequency use," *IEEE Trans. Magn.* **41**(10), 3262–3264 (2005).
- J. Lou, R. E. Insignares, Z. Cai, K. S. Zierner, M. Liu, and N. X. Sun, "Soft magnetism, magnetostriction, and microwave properties of FeGaB thin films," *Appl. Phys. Lett.* **91**(18), 182504 (2007).
- X. Liang, C. Dong, H. Chen, J. Wang, Y. Wei, M. Zaeimbashi, Y. He, A. Matyushov, C. Sun, and N. Sun, "A review of thin-film magnetoelastic materials for magnetoelectric applications," *Sensors* **20**(5), 1532 (2020).
- J. Wang, C. Dong, Y. Wei, X. Lin, B. Athey, Y. Chen, A. Winter, G. M. Stephen, D. Heiman, Y. He, H. Chen, X. Liang, C. Yu, Y. Zhang, E. J. Podlaha-Murphy, M. Zhu, X. Wang, J. Ni, M. McConney, J. Jones, M. Page, K. Mahalingam, and N. X. Sun, "Magnetostriction, soft magnetism, and microwave properties in Co-Fe-C alloy films," *Phys. Rev. Appl.* **12**(3), 034011 (2019).
- W. Yu, J. A. Bain, W. C. Uhlig, and J. Unguris, "The effect of stress-induced anisotropy in patterned FeCo thin-film structures," *J. Appl. Phys.* **99**(8), 08B706 (2006).
- P. Zou, W. Yu, and J. A. Bain, "Influence of stress and texture on soft magnetic properties of thin films," *IEEE Trans. Magn.* **38**(5), 3501–3520 (2002).
- D. Sander, "The correlation between mechanical stress and magnetic anisotropy in ultrathin films," *Rep. Prog. Phys.* **62**(5), 809 (1999).
- D. Lordan, G. Wei, P. McCloskey, C. O'Mathuna, and A. Masood, "Origin of perpendicular magnetic anisotropy in amorphous thin films," *Sci. Rep.* **11**(1), 3734 (2021).
- D. Z. Bai, J. G. Zhu, W. Yu, and J. A. Bain, "Micromagnetic simulation of effect of stress-induced anisotropy in soft magnetic thin films," *J. Appl. Phys.* **95**(11), 6864–6866 (2004).
- D. W. Hoffman, "Perspective on stresses in magnetron-sputtered thin films," *J. Vac. Sci. Technol. A* **12**(4), 953 (1994).

- <sup>25</sup>H. Windischmann, "Intrinsic stress in sputtered thin films," *J. Vac. Sci. Technol. A* **9**(4), 2431 (1991).
- <sup>26</sup>Y. Shimada and H. Kojima, "Sputtering of amorphous Co-Zr and Co-Hf films with soft magnetic properties," *J. Appl. Phys.* **53**(4), 3156 (1982).
- <sup>27</sup>S. Li, M. Liu, F. Xu, J. Lou, Z. Tian, J. Wu, Y. Hu, X. Cai, J. G. Duh, and N. X. Sun, "Soft magnetism and microwave magnetic properties of Fe-Co-Hf films deposited by composition gradient sputtering," *J. Appl. Phys.* **109**(7), 07A315 (2011).
- <sup>28</sup>S. Li, Z. Huang, J. G. Duh, and M. Yamaguchi, "Ultrahigh-frequency ferromagnetic properties of FeCoHf films deposited by gradient sputtering," *Appl. Phys. Lett.* **92**(9), 092501 (2008).
- <sup>29</sup>H. W. Chang, Y. H. Huang, C. C. Hsieh, C. W. Shih, W. C. Chang, and D. S. Xue, "Study on the soft magnetic properties and high frequency characteristics of Co-M (M = Ti, Zr, and Hf) thin films," *J. Appl. Phys.* **111**(7), 07A333 (2012).
- <sup>30</sup>G. G. Stoney, "The tension of metallic films deposited by electrolysis," *Proc. R. Soc. London, Ser. A* **82**(553), 172–175 (1909).
- <sup>31</sup>P. T. Brewick, S. I. Wright, and D. J. Rowenhorst, "NLPAR: Non-local smoothing for enhanced EBSD pattern indexing," *Ultramicroscopy* **200**, 50–61 (2019).
- <sup>32</sup>J. Betz, K. Mackay, J. C. Peuzin, D. Givord, and B. Halstrup, "Giant magnetostrictive, spring magnet type multilayers and torsion based microactuators," *MRS Proc.* **459**(1), 571–576 (1996).
- <sup>33</sup>E. du Trémolet de Lacheisserie and J. C. Peuzin, "Magnetostriction and internal stresses in thin films: The cantilever method revisited," *J. Magn. Magn. Mater.* **136**(1–2), 189–196 (1994).
- <sup>34</sup>Y. Huo, S. Sofronici, X. Wang, M. J. D'Agati, P. Finkel, K. Bussmann, T. Mion, M. Staruch, N. J. Jones, B. Wheeler, K. L. McLaughlin, M. G. Allen, and R. H. Olsson, "Low noise, strain modulated, multiferroic magnetic field sensor systems," *IEEE Sens. J.* **23**(13), 14025–14040 (2023).